Ground states, energy landscape and low-temperature dynamics of $\pm J$ spin glasses

S. Kobe[1] and J. Krawczyk[1,2]
[1]Institut für Theoretische Physik, Technische Universität Dresden, D-01062 Dresden, Germany
[1,2]ARC Centre of Excellence for Mathematics and Statistics of Complex Systems, The University of Melbourne, Parkville Victoria 3010, Australia

November 23, 2004

1 Introduction

The previous three chapters have focused on the analysis of computational problems using methods from statistical physics. This chapter largely takes the reverse approach. We turn to a problem from the physics literature, the spin glass, and use the branch-and-bound method from combinatorial optimization to analyze its energy landscape. The spin glass model is a prototype that combines questions of computational complexity from the mathematical point of view and of glassy behavior from the physical one. In general, the problem of finding the ground state, or minimal energy configuration, of such model systems belongs to the class of NP-hard tasks.

The spin glass is defined using the language of the Ising model, the fundamental description of magnetism at the level of statistical mechanics. The Ising model contains a set of n spins, or binary variables S_i, each of which can take on the value "up" ($S_i = 1$) or "down" ($S_i = -1$). Finding the ground state means finding the spin variable values minimizing the Ising Hamiltonian energy (cost) function, written in general as

$$E = -\sum_{i<j}^{n} J_{ij}\, S_i\, S_j \tag{1}$$

for given interaction strengths J_{ij}. This is a problem of nonlinear discrete optimization. When J_{ij} is positive, interactions are called *ferromagnetic*. In this case, there is a trivial solution: all spins are aligned, meaning they have identical sign. When J_{ij} is negative, interactions are called *antiferromagnetic*. Physically, the spins are often taken to lie on a lattice. For a square or cubic lattice with negative J_{ij} for neighboring pairs of spins and $J_{ij} = 0$ otherwise, the ground state is clearly the configuration where adjacent spins have opposite sign.

If all nonzero interaction strengths J_{ij} are equal, the system is said to be *ordered*. For ordered systems with antiferromagnetic interactions between nearest neighbors, but where neighbors of a given spin are also neighbors of each other, *frustration* prevents certain interactions from being "satisfied." An example is the triangular lattice: to quote the early work of Wannier, "antiferromagnetism does not fit into the triangular pattern" [1]. While the solution to the optimization problem is straightforward, one third of all interactions lead to conflicts that increase the ground-state energy. The structural sensitivity of antiferromagnetic order has been discussed by Sato and Kikuchi [2] for the face-centered cubic lattice. Other ordered systems have been considered by Liebmann [3].

The problem becomes more complex when *disorder* arises, and interaction strengths are not equal. Often, such systems can only be solved by numerical methods. The time complexity of an algorithm is defined by the growth of the solution time as a function of input size [4]. For many disordered spin models, it can be shown that finding ground states is NP-hard [5, 6], and so the time complexity likely grows faster than any polynomial. In order to address this, Kobe and Handrich [7] introduced a "misfit" parameter characterizing the degree of frustration, and used it to find exact ground states in a two-dimensional system of $n = 23$ hard disks (an amorphous Ising model) with distance-dependent antiferromagnetic interactions. Further exact results for two-dimensional ($n = 40$) and three-dimensional systems ($n = 30$) were obtained by Kobe [8, 9] using the branch-and-bound method of combinatorial optimization [10].

Another concept for studying systems with disorder and competing interactions was introduced by Toulouse [11]. He analyzed the frustration effect in a two-dimensional lattice model with a random distribution of ferromagnetic and antiferromagnetic nearest-neighbor interactions J_{ij} of equal strength, known as the Edwards-Anderson $\pm J$ model. The system may be described by plaquettes representing elementary lattice regions, such as a unit cell on

a square lattice. The quantity $\Phi = \prod_c J_{ij}$, taken over the contour c forming the perimeter of the plaquette, measures frustration: $\Phi = -1$ if the plaquette is frustrated, $\Phi = 1$ if it is not. The exact ground state is then associated directly with a matching [12] of frustrated plaquettes that minimizes the sum of lattice distances between matched pairs. The multiplicity of ground states, or degeneracy, comes from the total number of ways to create such a minimal matching. This approach only works for two-dimensional systems, but it is an efficient one, since minimal matching can be solved to optimality in polynomial time. In the years following Toulouse's work, the matching method of optimization was used widely [13, 14].

This chapter is organized as follows. In Section 2, we introduce the branch-and-bound algorithm as a prototype for a numerical procedure of nonlinear discrete optimization. Then, in Section 3, we describe the Edwards-Anderson $\pm J$ spin glass model and give an overview of numerical results for the ground-state energy and entropy. In Section 4 the low-energy landscape of finite three-dimensional $\pm J$ spin glasses (consisting of clusters and valleys) is analyzed and visualized. The correlation with the real-space picture shows the existence of rigid spin domains in the ground state. We discuss dynamical consequences in Section 5, focusing on the transition from one ground-state cluster to another by way of a saddle cluster. It can be shown that internal structure contributes to the slowing of relaxation processes. Finally, we point out the progress and challenges of complexity theory for a better microscopic understanding of glassy behavior.

2 Branch-and-bound

The ground state of the Ising model with n spins $S_i = \pm 1$ is the spin configuration with energy

$$E_0 = \min_{S_i = \pm 1} \left(- \sum_{i<j}^{n} J_{ij} \, S_i \, S_j \right) . \tag{2}$$

For interactions J_{ij} of arbitrary sign and magnitude, finding the exact ground state is an NP-hard problem. Since the number of states increases with 2^n, only for very small n can Eq. (2) be solved by complete enumeration.

Complete algorithms for combinatorial optimization problems aim to reduce the numerical effort while still giving an exact solution. The general

principle can be demonstrated for the branch-and-bound algorithm. The strategy of branch-and-bound is to exclude as many states with high energy values as possible, in an early stage of calculation [9]. Let us consider a small cluster with $n = 8$ spins and J_{ij} values of differing strengths. To simplify matters and without loss of generality, we take the case where there are only antiferromagnetic interactions, representing an amorphous antiferromagnetic cluster with dilution. The upper triangle of the interaction matrix $\mathbf{J} = (J_{ij})$ is given by

$$\mathbf{J} = \begin{pmatrix} 0 & -5 & -2 & -5 & -6 & -1 & 0 & 0 \\ & 0 & -10 & -4 & 0 & -2 & -1 & 0 \\ & & 0 & 0 & 0 & -3 & 0 & -1 \\ & & & 0 & -3 & -5 & -7 & -4 \\ & & & & 0 & -4 & -5 & -8 \\ & & & & & 0 & 0 & -1 \\ & & & & & & 0 & 0 \\ & & & & & & & 0 \end{pmatrix} . \tag{3}$$

In Fig. 1, a tree is constructed by successively fixing spin values. At the branching depth $l = 1$, spin number 1 is set to the positive direction (+). At depth $l = 2$ the spin number 2 is fixed, and so on. At each branching node a configuration $(S_1, ..., S_l)$ and an energy value E_l is shown. For $l = 1$ the starting energy $E_1 = E_{id}$ is chosen, where $E_{id} = -\sum_{i<j} |J_{ij}|$ is a lower bound on the ground-state energy E_0 in Eq. (2), representing the situation where all interactions are satisfied and no conflict is present. The other values E_l for $1 < l \leq n$ can be obtained by the following rule:

$$E_l = E_{l-1} + 2 \sum_{k(\|l)}^{l-1} |J_{kl}|. \tag{4}$$

In the example of Eq. (3), where all interactions are antiferromagnetic, $k(\|l)$ denotes those k for which spin k has already been fixed in the same direction as the spin l. More generally, when both positive and negative J_{ij} values are present, the sum contains those contributions that arise due to conflicts of spin l with all spins fixed earlier. In Fig. 1 the values of the summation term in Eq. (4) are given at the branching lines. From Eq. (4) it follows that

$$E_l \geq E_{l-1}. \tag{5}$$

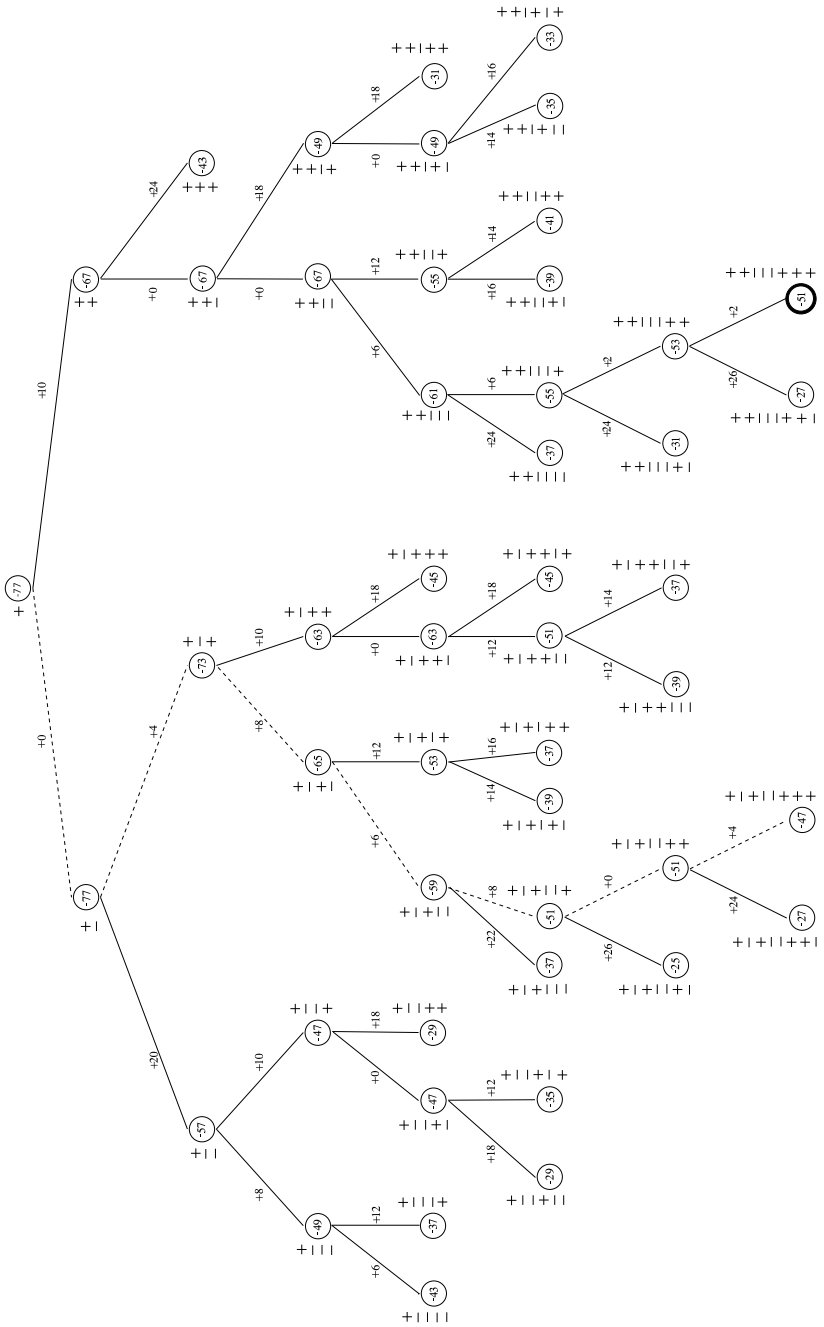

Figure 1: Branch-and-bound tree for a cluster with $n = 8$ spins given by the interaction matrix $\mathbf{J}$ in Eq. (3); $E_{id} = -77$, $E_{bound} = -47$ obtained by steepest descent (dashed line). The exact ground state with the energy $E_0 = -51$ is marked in bold.

It is easy to recognize that all configurations of the system (modulo a global spin flip) and their associated energies can be found at the bottom of the fully branched tree, at $l = n$. The goal of the branch-and-bound strategy is to prune some branches. In order to do this, a heuristic is used to generate an approximate solution, e.g., the greedy procedure of steepest descent shown in Fig. 1 where at each step the new contribution to the sum in Eq. (4) is minimized. In our example, the energy of the resulting configuration is -47. This value is used as E_{bound}, and signals that branching can stop at any node where $E_l > E_{bound}$. From Eq. (5) it is certain that all branches pruned in this way can lead only to states with $E_n \geq E_{bound}$, and so none of them can yield a solution to Eq. (2). Therefore, in place of a complete enumeration of all states, the pruned tree in Fig. 1 can be used to search for E_0. Ultimately, either the ground state is found with $E_0 < E_{bound}$, or it can be proven that the heuristic solution was already the exact ground state. The reduction of numerical effort is already obvious for the small example of Fig. 1: 49 nodes are calculated rather than 128 states in the case of complete enumeration. The increase of CPU time with system size is estimated to be $t_{calc} = 2^{\alpha n}$, with $\alpha = 0.23$ and 0.27 for the determination of all ground states of $\pm J$ spin glasses on square and simple cubic lattices respectively [15].

It should be mentioned that the algorithm also yields *all* low-lying states with energies lower than E_{bound}, if $E_{bound} > E_0$ is chosen. This variant of the algorithm is used in Section 4 to construct the complete energy landscape.

3 Ground-state energy and entropy of the $\pm J$ spin glass: numerical results

In the preceding section we have given an example of applying numerical methods of nonlinear discrete optimization to determine the ground state E_0 (Eq. (2)). In this section and in the following ones, we will concentrate on a special case, the Edwards-Anderson $\pm J$ model. Here, interactions are between nearest neighbors on a hypercubic lattice, they are of equal strength ($|J_{ij}| = J$ for all neighboring spins i and j), and their signs are random. We impose $\sum_{i<j}^{n} J_{ij} = 0$ for each realization of the system, so that there is an equal number of ferromagnetic and antiferromagnetic interactions. We first present a survey of the best numerical results obtained by exact optimization algorithms [16]. Besides branch-and-bound, these include the branch-and-cut

method [6] based on rewriting the quadratic energy function in Eq. (2) with additional inequalities that must hold for feasible solutions. The practical challenge here is that not all necessary inequalities are known a priori, and can arise during the iteration procedure [4, 17, 18]. Their number grows

Table 1: Ground-state energy per spin e_0 and entropy per spin s_0 of the hypercubic $\pm J$ spin glass in d dimensions. Results for infinite systems are extrapolated from system sizes up to $n = L_{max}^d$. Parenthetical numbers denote error bar in final digit(s).

d	method	L_{max}	e_0	s_0	ref.
2	matching*	1800	-1.40193(2)		[19]
2	branch-and-cut	50	-1.4015(8)		[18]
2	branch-and-bound	8	-1.40(6)	0.077(21)	[15]
2	genetic cluster appr.	40	-1.4015(3)		[20]
	genetic cluster appr.	40		0.078(5)	[21]
2	transfer matrix×	11	-1.4024(12)	0.0701(5)	[22]
2	expansion-fall-invasion-spring	10	-1.40169		[23]
2	genetic	20	-1.401(1)		[24]
2	flat histogram sampling	32	-1.4007(85)	0.0709(6)	[25]
3	branch-and-bound	4	-1.778(14)	0.054(16)	[15]
3	extremal optimization	12	-1.7865(3)		[26]
3	genetic	10	-1.787(3)		[24]
	genetic cluster appr.	8		0.051(3)	[21]
3	genetic cluster appr.	14	-1.7876(3)		[4]
3	multicanonical sampling	12		0.04412(46)	[27]
4	genetic cluster appr.	7	-2.095(1)		[4]
	genetic cluster appr.	6		0.027(5)	[21]
4	extremal optimization	7	-2.093(1)		[26]
5	extremal optimization+	4	-2.3511		[28]

* free boundary conditions

× rectangular lattice ($L \times W$) with $L_{max} = 11$ (periodic boundary conditions) and $W_{max} = 10^4 \cdots 10^5$ (free boundary conditions)

+ without extrapolation

exponentially with the system size.

In Table 1, the ground-state energy per spin for hypercubic systems of different dimensions are given, in the asymptotic limit of an infinite system. These results are extrapolated from finite-size numerics. The "world record" in system size for an exact solution is obtained using the matching method for a two-dimensional system with free boundary conditions up to $n = 1800 \times 1800$ [19]. Of course, since minimal matching can be solved in polynomial time, the complexity for this version of the problem is comparatively low. For higher dimensions, Table 1 includes results coming both from exact and from approximation methods. The accuracy of approximation methods is in many cases supported by exact values obtained for smaller system sizes than the maximum shown here. As they are incomplete methods, it is generally impossible to supply any further evidence for their exactness [4]. However, the inclusion of such methods with a "high level of reliability" [29] provides the possibility of considering systems of larger size than would be otherwise available, and thus to extrapolate more convincingly to infinite lattices. Much less is known about the exact ground-state energy for other than hypercubic lattices.

A shortcoming of presenting the ground-state energy per spin is that the value is not comparable across different dimensions, lattice types, etc. For that reason, a universal measure of frustration has been introduced by the *misfit* parameter

$$\mu_0 = \frac{1}{2}\left(1 + \frac{E_0}{\sum_{i<j} |J_{ij}|}\right), \tag{6}$$

representing the mean fraction of unsatisfied bonds in the ground state [30]. For the $\pm J$ spin glass, μ_0 values from numerical simulations are compiled in Table 2. They may be compared with $\mu_0 = 1/3$ for the antiferromagnetic triangular or face-centered cubic lattice, and $\mu_0 = 1/2$ for fully frustrated hypercubic and face-centered cubic lattices in the limiting case of infinite dimensions [32, 33]. Moreover, it can be seen that the $\pm J$ spin glass is less frustrated on the honeycomb lattice, and more frustrated on the triangular lattice, than on the square one.

Table 2: Misfit parameter μ_0 of the $\pm J$ spin glass in d dimensions. Estimate for infinite system, extrapolated from numerics.

lattice	d	μ_0	E_0 from
honeycomb	2	0.09	[31]
square	2	0.150	Table 1
triangular	2	0.22	[31]
simple cubic	3	0.202	Table 1
hypercubic	4	0.24	[26]
hypercubic	5	0.26	[28]

4 Energy landscape

An advantage of the branch-and-bound algorithm is that it is very easy to implement a variant allowing the calculation of all near-optimal solutions. For these purposes, a certain $E_{bound} > E_0$ has to be chosen and fixed during the calculation. All states of the system with energy $E_i < E_{bound}$ can then be found. (Note that here, the subscript i denotes an excited state of the system, i.e., with higher energy than the ground state, rather than an intermediate level of branch-and-bound as in Section 2.) Through subsequent analysis of these states with respect to their neighborhood structure, the complete low-energy landscape in the high-dimensional configuration space can be obtained. The situation in this space is analgous to that of "fog in the mountains" in a real landscape: all areas below the upper limit of the fog are covered.

Let us first investigate the low-energy landscape of a three-dimensional system of size $n = 4 \times 4 \times 4$, with periodic boundary conditions. All $N = 1635796$ configurations up to the third excitation (fourth-lowest energy state) were calculated using branch-and-bound [34]. The configurations were then studied with regard to their one-spin neighborhood. Two configurations that differ in the orientation of only one spin are considered neighbors. Consequently, each of the N configurations can have at most n neighbors belonging to the set of N. The low-energy landscape is formed by all states of energy E_k, with $k \leq 3$. Due to the discreteness of the coupling constants J_{ij}, the energy values are degenerate. E_0 is the ground-state energy and

$E_k = E_0 + 4k$ are the excitation energies.

An energy landscape is thus formed, consisting of clusters, valleys and saddles [35, 36, 37]. A set of configurations is called a *cluster* if a "chain" connecting them exists. The chain is built up by neighboring configurations with the same energy. The landscape is symmetric, due to Eq. (2). Two clusters of different energies are *connected* whenever at least one configuration of the first cluster is a neighbor of one configuration of the second cluster. A schematic picture of this low-energy landscape is illustrated in Fig. 2. Finally, *valleys* can be associated with ground-state clusters. A valley consists of clusters that have connections to one single ground-state cluster. Different valleys are connected by *saddle* clusters, which mediate the transition over energy barriers.

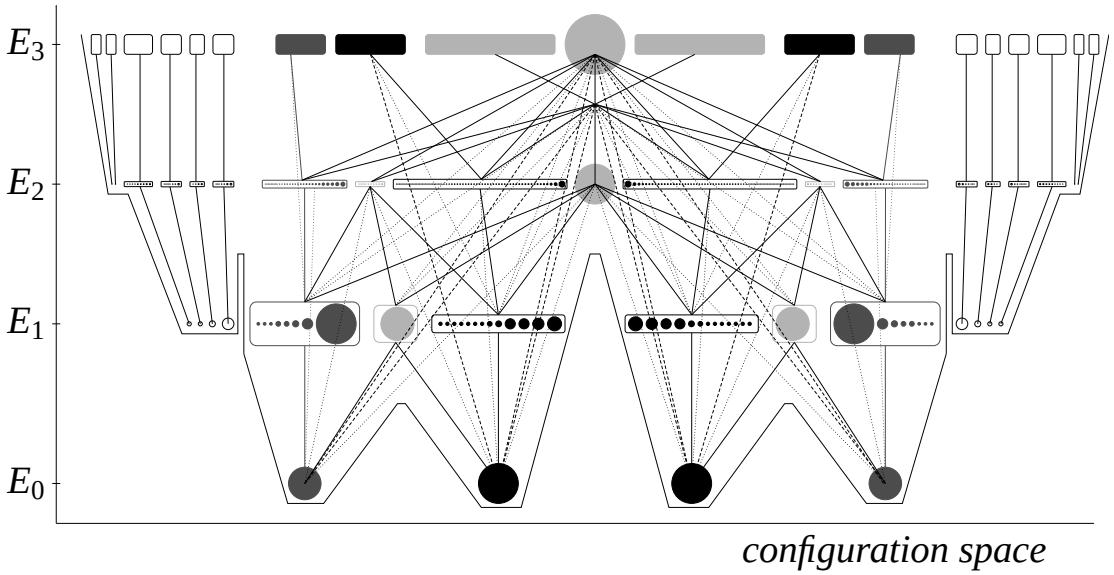

Figure 2: Schematic picture of the exact low-energy landscape up to the third excitation. Clusters are marked by circles of size proportional to the number of configurations in the cluster: the two ground-state clusters on the left, for instance, consist of 12 and 18 configurations. (Note that the scale is different for different energy levels, so the largest cluster in the first, second and third excitation contains 819, 82960 and 1503690 configurations, respectively). Lines denote single spin-flip connections. All clusters connected to the same neighborhood structure are pooled in a box.

Table 3: Characteristic properties of the ground states for 8555 realizations of systems of size $n = 4 \times 4 \times 4$. N_{sys} denotes the number of systems, $\overline{s}_0$ the mean ground-state entropy, $\overline{N}_{Cl}$ the mean number of clusters, and $\overline{N}_{GS}$ the mean number of ground states.

E_0	N_{sys}	$\overline{s}_0$	$\overline{N}_{Cl}$	$\overline{N}_{GS}$
-100	5	0.1153 ± 0.0091	10.20 ± 2.82	3848
-104	505	0.0974 ± 0.0231	6.19 ± 3.14	1088
-108	2769	0.0748 ± 0.0257	3.19 ± 1.99	326
-112	3541	0.0566 ± 0.0249	1.91 ± 1.17	114
-116	1358	0.0448 ± 0.0221	1.38 ± 0.74	45
-120	291	0.0371 ± 0.0210	1.18 ± 0.46	24
-124	52	0.0311 ± 0.0181	1.11 ± 0.32	14
-128	7	0.0259 ± 0.0235	1.33 ± 0.57	41
	8555	0.0623 ± 0.0285	2.47 ± 1.98	228

Note that there is a broad distribution of realizations of the $\pm J$ systems.

Table 4: Characteristic properties of the first excitations for 8555 realizations of systems of size $n = 4 \times 4 \times 4$. $\overline{N}_1$ denotes the mean number of first excited states, $\overline{N}_{cl1}$ the mean number of clusters, $\overline{N}_s$ the mean number of saddle states, $\overline{N}_{cls}$ the mean number of saddle clusters, $\overline{N}_m$ the mean number of metastable states, and $\overline{N}_{clm}$ the mean number of metastable clusters.

E_0	$\overline{N}_1$	$\overline{N}_{cl1}$	$\overline{N}_s$	$\overline{N}_{cls}$	$\overline{N}_m$	$\overline{N}_{clm}$
-100	384825	61.00 ± 8.51	191598	0.70 ± 0.45	351	7.20 ± 3.56
-104	102879	47.64 ± 15.76	50016	0.98 ± 0.68	543	6.31 ± 3.58
-108	25469	33.48 ± 14.37	11079	0.99 ± 0.90	375	4.59 ± 2.73
-112	6653	23.02 ± 10.81	2199	0.54 ± 0.77	151	2.57 ± 1.98
-116	1895	17.01 ± 7.76	375	0.30 ± 0.62	42	1.25 ± 1.28
-120	775	14.18 ± 5.07	81	0.16 ± 0.41	14	0.59 ± 0.94
-124	395	12.81 ± 4.11	22	0.15 ± 0.44	2	0.14 ± 0.36
-128	322	13.42 ± 4.75	13	0.14 ± 0.38	0.43	0.14 ± 0.37
	17634	26.5 ± 14.4	7326	0.68 ± 0.83	225	3.14 ± 2.73

The ground-state energy of 8555 systems of the size $n = 4 \times 4 \times 4$ varies between E_0 = -100 and -128. The respective values for the mean ground-state entropy $\overline{s}_0$, number of clusters $\overline{N}_{Cl}$ and number of ground states $\overline{N}_{GS}$ are given in Table 3.

In Table 4 corresponding values characterizing the structure of the first excitations of the same set of realizations are given. Here, the following average values are specified: $\overline{N}_1$ is the number of states in the first excitation: of these, $\overline{N}_s$ belong to saddle clusters and $\overline{N}_m$ are metastable states without direct connections to one of the ground states. $\overline{N}_{cl1}$ is the number of clusters: of these, $\overline{N}_{cls}$ are saddle clusters and $\overline{N}_{clm}$ are metastable clusters. It can be seen that systems with higher ground-state energies (i.e., higher frustration) also possess a more complex energy landscape with larger entropy and many clusters.

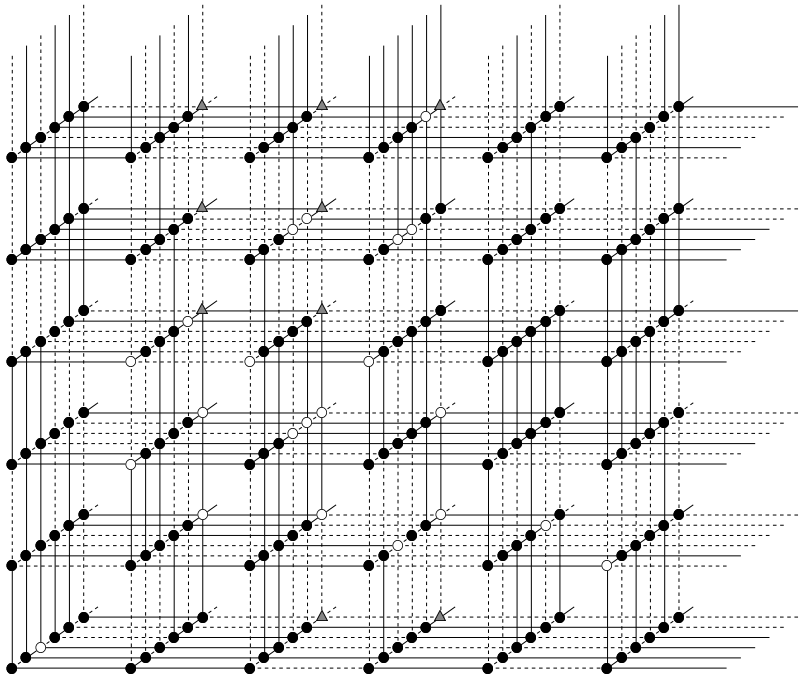

Figure 3: Two spin domains of a $\pm J$ spin glass with $n = 6 \times 6 \times 6$, marked by full circles and shaded triangles. All spins that are free in either of the ground-state clusters are marked by empty circles.

The relation between the energy landscape in configuration space and the spin structure in real space is demonstrated in Fig. 3. Here an example with $n = 6 \times 6 \times 6$ spins is shown. The ground states can be grouped into four clusters, similar to the situation of Fig. 2. Two clusters contain 5632 states and two clusters contain 1280 states. The degeneracy within the clusters is caused by the existence of "free spins" that feel no internal field and can thus be flipped without energy input. Let us first consider the two clusters that remain when one ignores the "mirror states" arising from a global spin flip. All spins in real space that are free in either of these clusters are marked by empty circles. The remaining spins are divided into two groups, marked by full circles and shaded triangles. In each of these groups the relative orientation of any given spin is fixed with respect to all others in the group. Due to this internal rigidity, the two groups are called "spin domains" [4]. When one includes the mirror states, there are four different orientations of the two spin domains, resulting in the four ground-state clusters in configuration space, see also [38]. Many of the free spins are situated physically between the spin domains. Thus, the low-energy excitations in Fig. 2 can be understood as a successive softening of the spin domains starting from the boundary region of free spins between them. Consequently, a transition over the saddle cluster with energy E_1 may be interpreted as a gradual process of reversal of one spin domain with respect to the other, one single spin flip at a time. By flipping spins, additional free spins are continually created and deleted: that is the mechanism driving this process [4, 39].

5 Dynamics

The complete knowledge of the low-energy landscape allows us to investigate the influence that the size of clusters and valleys and their neighborhood structure have on dynamics [40]. The time evolution of the system in configuration space can be described as the progressive exploration of clusters and valleys. We use the Monte Carlo Metropolis algorithm with various values of $\beta = 1/\tau$, where τ is the temperature of the heat bath [41]. One Monte Carlo step (MCS) is taken as the time unit. An individual run through the landscape is shown in Fig. 4. We start from an arbitrary state in the leftmost ground-state cluster of Fig. 2.

At first, the system walks in the valley, sometimes touching the saddle cluster in the first excitation. After an escape time t_{esc} of the order of 10^7

MCS, the system leaves the first valley and goes through the saddle cluster to the second one. This transition is governed by the internal structure of the saddle cluster, shown as its transition profile in Fig. 5. First, all pairs of configurations are checked to find the largest Hamming distance h_d (the number of spin values differing between the two configurations). Then, using one of these states as the reference state, the h_d values of all configurations in the saddle cluster with respect to the reference state are calculated. Two sets of states are marked, one consisting of states connected by a single spin flip with the first valley and the other with the second valley. These sets denote the input and the output areas for a transition from one valley to the other. Considering a transition as a walk between these sets, it is clearly slowed down by the small numbers of states in between.

Quantitatively, the random walk can be described by the spin correlation

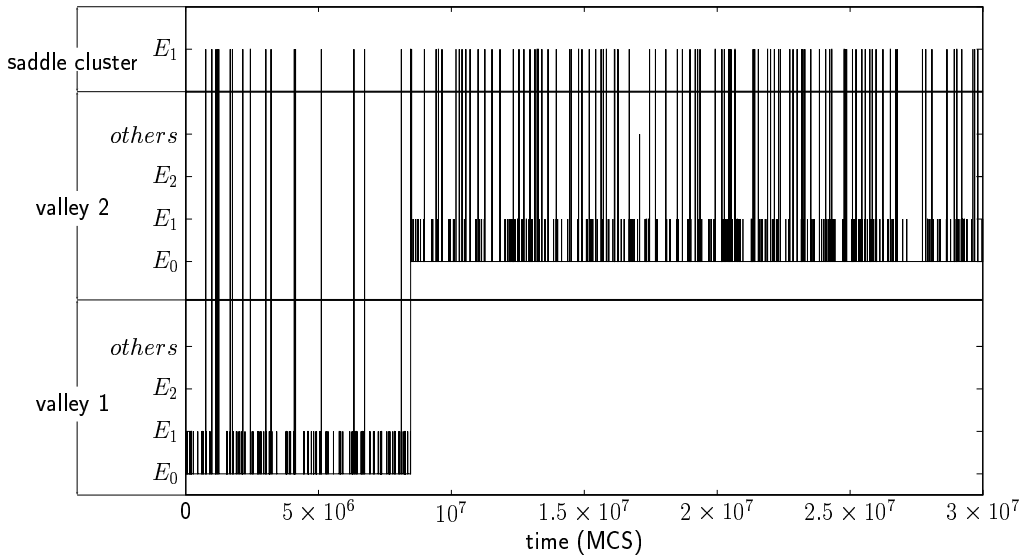

Figure 4: An individual Monte Carlo run through the landscape vs. time, at inverse temperature $\beta = 2.5$. The process starts from an arbitrary state within the ground-state cluster on the left in Fig. 2. The vertical axis shows different energies belonging to valleys #1 and #2, respectively, and the energy E_1 of the saddle cluster connecting both ground-state clusters within the first excitation.

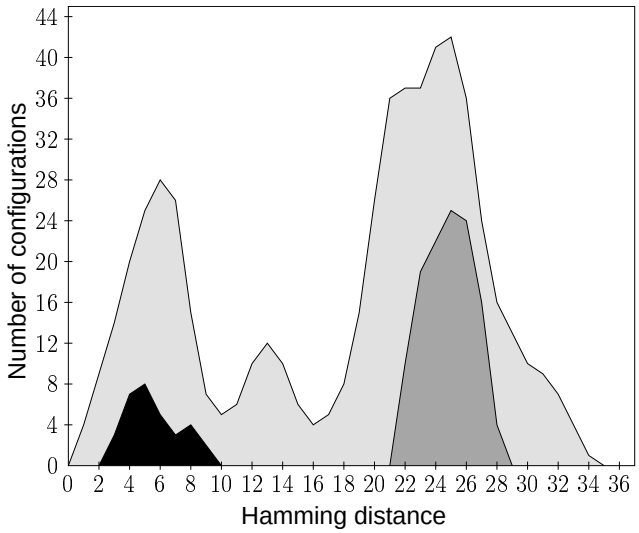

Figure 5: The transition profile of the saddle cluster illustrated by the number of configurations vs. Hamming distance from a reference state (see text). The shaded area marks all configuration in the saddle cluster. States having connections with valley #1 (dark) and #2 (middle) are shown in black and grey respectively.

function

$$q(t) = \frac{1}{n}\left\langle \sum_{i=1}^{n} S_i^G(0) S_i(t) \right\rangle, \tag{7}$$

where $S_i^G(0)$ is the ith spin of the starting configuration chosen arbitrarily from the ground states of valley #1 or #2. The brackets denote the average of 100 runs starting from the same state (Fig. 6).

The spin correlation function $q(t)$ vs. time is characterized by a plateau with the value q_{pl} followed by a temperature-dependent decay. It should be noted that such a plateau is typical for supercooled liquids, where the dynamical process is called α-relaxation. To examine the correlation between the structure of the landscape and the dynamics, we compare q_{pl} with the size of the valley, keeping in mind that the spin correlation within the valley can be calculated using the mean Hamming distance $\overline{h}_d$ of all pairs of states by

$$q_{pl}^{(Ham)} = 1 - 2\overline{h}_d/n. \tag{8}$$

We find an agreement between q_{pl} and $q_{pl}^{(Ham)}$ (Table 5), where the average in

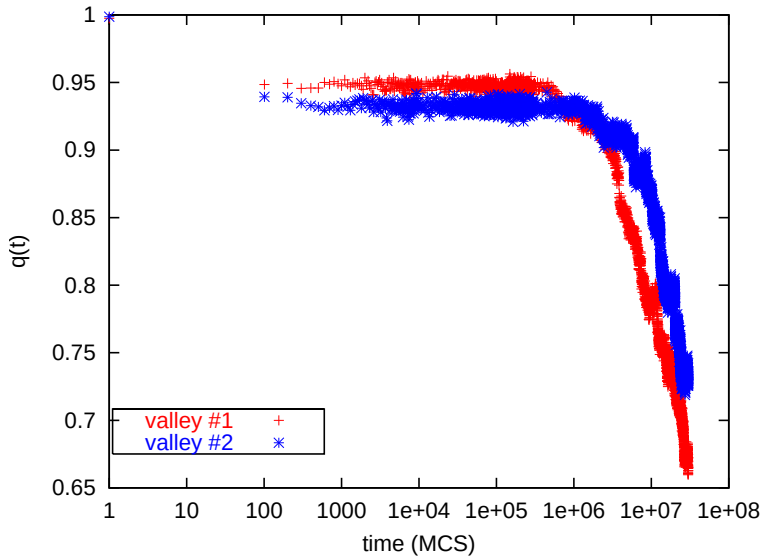

Figure 6: The spin correlation function vs. time. The starting configuration is selected from the set of ground states of valley #1 and #2. The Monte Carlo process is run at inverse temperature $\beta = 2.5$.

Eq. (8) is approximated by the average over all states in the corresponding ground state clusters.

The plateau thus reflects the dynamics within the valley. The subsequent decay of $q(t)$ shows the escape from the valley. The escape time t_{esc} depends on the temperature and can be fitted by $t_{esc} \sim exp(\beta\ \Delta E_{eff})$. We found $\Delta E_{eff} = 4.24 \pm 0.08$ for valley #1 and $\Delta E_{eff} = 4.46 \pm 0.09$ for valley #2. The effective energy barrier is larger than the real one, which is $\Delta E = E_1 - E_0 = 4$ in our example. Moreover, ΔE_{eff} is larger for valley #2 than for #1. This reflects the fact that the system can leave the saddle cluster more easily in

Table 5: The values of q_{pl} obtained from simulations (Fig. 6) and calculation (Eq. (8))

	Fig. 6	Eq. (8)
q_{pl} (#1)	0.947 ± 0.004	0.936
q_{pl} (#2)	0.932 ± 0.004	0.924
Δq_{pl}	0.015 ± 0.004	0.012

the direction of #2, as there are more exit connections (see Fig. 5).

6 Summary

Due to the physical complexity of the spin glass problem, advanced methods of combinatorial optimization are required. In recent years, powerful numerical algorithms have become available, enabling us to study model systems of small and moderate sizes from the microscopic point of view. For example, it is possible to determine the internal structure of an energy landscape in a high-dimensional configuration space. Understanding the slow dynamics of glassy systems is a current challenge of solid state physics. Spin glasses are good candidates for modeling glassy behavior.

In this chapter, we have discussed the $\pm J$ spin glass model, and shown the correlation between the microscopic structure of the energy landscape and the dynamical behavior. The characteristic shape of the correlation function may be attributed to the restricted connectivity of clusters and valleys in the energy landscape and to their internal profiles. Finding better algorithms for NP-hard problems remains an ongoing challenge. Our hope is that with the development of improved algorithms, the restriction to small system sizes can be eased, and the ground-state behavior of $\pm J$ spin glasses can be analyzed with improved confidence [42].

7 Acknowledgements

The authors wish to thank A. Heuer, S. Boettcher and A.K. Hartmann for valuable discussions, and the latter for permission to use his data concerning the ground state of a three-dimensional system with $L = 6$. This work has been supported by Graduiertenkolleg "Struktur- und Korrelationeffekte in Festkörpern".

References

[1] G. H. Wannier, Phys. Rev. 79, 357 (1950)

[2] H. Sato, R. Kikuchi, in: AIP Conf. Proc. No. 18, Part 1, Magnetism and Magnetic Materials, 1973, ed. C. D. Graham, Jr. and J.J. Rhyne, AIP, New York (1974), p. 605

[3] R. Liebmann, Statistical Mechanics of Periodic Frustrated Ising Systems, Lecture Notes in Physics, Vol. 251, Springer-Verlag Berlin, 1986

[4] A. K. Hartmann, H. Rieger, Optimization algorithms in physics, Wiley-VHC Verlag Berlin, 2002

[5] F. Barahona, J. Phys. A: Math. Gen. 15, 3241 (1982)

[6] M. Grötschel, M. Jünger, G. Reinelt, in: Heidelberg Colloquium on Glassy Dynamics, ed. J. L. van Hemmen and I. Morgenstern, Lecture Notes in Physics, Vol. 255, Springer-Verlag Berlin, 1987, p. 325

[7] S. Kobe, K. Handrich, phys. stat. sol. (b) 73, K65 (1976)

[8] S. Kobe, in: Amorphous Magnetism II, ed. R. A. Levy and R. Hasegawa, Plenum Press, New York and London (1977), p. 529

[9] S. Kobe, A. Hartwig, Comput. Phys. Commun. 16, 1 (1978)

[10] W.L. Eastman, "Linear programming with pattern constraints," Ph.D. thesis, Computation Laboratory, Harvard University, Cambridge, MA (1958); A.H. Land and A.G. Doig, "An Automatic Method for Solving Discrete Programming Problems," Econometrica 28, 497-520 (1960); J.D.C. Little, K.G. Murty, D.W. Sweeney, C. Karel, "An Algorithm for the Traveling-Salesman Problem," Operations Research 11, 972-989 (1963)

[11] G. Toulouse, Communications on Physics 2, 115 (1977)

[12] J. Edmonds, J. Res. Nat. Bureau Standards 69B, 125 (1965)

[13] I. Bieche, R. Maynard, R. Rammal, J. P. Uhry, J. Phys. A: Math Gen. 13, 2553 (1980)

[14] F. Barahona, R. Maynard, R. Rammal, J. P. Uhry, J. Phys. A: Math. Gen. 15, 673 (1982)

[15] T. Klotz, thesis, Technische Universität Dresden, 1996

[16] D. Stauffer, Physics World, May 1999, p. 23

[17] C. De Simone, M. Diehl, M. Jünger, P. Mutzel, G. Reinelt, G. Rinaldi. J. Stat. Phys. 80, 487 (1995)

[18] C. De Simone, M. Diehl, M. Jünger, P. Mutzel, G. Reinelt, G. Rinaldi. J. Stat. Phys. 84, 1363 (1996)

[19] R. G. Palmer, J. Adler, Int. J. Mod. Phys. C 10, 667 (1999)

[20] A. K. Hartmann, Eur. Phys. J. B 8, 619 (1999)

[21] A. K. Hartmann, Phys. Rev. E 63, 016106 (2001)

[22] H.-F. Cheung, W. McMillan, J. Phys. C: Solid State Phys. 16, 7027 (1983)

[23] E. E. Vogel, A.J. Ramirez-Pastor, F. Nieto, Physica A 310, 384 (2002)

[24] U. Gropengiesser, J. Stat. Phys. 79, 1005 (1995)

[25] Z. F. Zhan, L. W. Lee, J.-S. Wang, Physica A 285, 239 (2000)

[26] S. Boettcher, A. G. Percus, Phys. Rev. Lett. 86, 5211 (2001)

[27] B. A. Berg, U. H. E. Hansmann, T. Celik, Phys. Rev. B 50, 16444 (1994)

[28] S. Boettcher, private communication

[29] J. Houdayer, O. C. Martin, Phys. Rev. E 64, 056704 (2001)

[30] S. Kobe, T. Klotz, Phys. Rev. E 52, 5660 (1995)

[31] W. Lebrecht, E. E. Vogel, Phys. Rev. B 49, 6018 (1994)

[32] B. Derrida, Y. Pomeau, G. Toulouse, J. Vannimenus, J. Phys. (Paris) 40, 617 (1979)

[33] S. Alexander, P. Pincus, J. Phys. A: Math. Gen. 13, 263 (1980)

[34] A. Hartwig, F. Daske, S. Kobe, Comput. Phys. Commun. 32, 133 (1984)

[35] T. Klotz, S. Kobe, J. Phys. A: Math. Gen. 27, L95 (1994)

[36] T. Klotz, S. Kobe, Acta Phys. Slovaca 44, 347 (1994)

[37] T. Klotz, S. Kobe, in: Hayashibara Forum '95, Int. Symp. Coherent Approaches to Fluctuations, Kyoto 1995, (M. Suzuki, N. Kawashima, eds.), World Scientific, Singapore 1996, p. 192.

[38] G. Hed, A. K. Hartmann, D. Stauffer, E. Domany, Phys. Rev. Lett. 86, 3148 (2001)

[39] E. E. Vogel, J. Cartes, P. Vargas, D. Altbir, S. Kobe, T. Klotz, M. Nogala, Phys. Rev. B 59, 3325 (1999)

[40] J. Krawczyk, S. Kobe, Physica A 315, 302 (2002)

[41] K. Binder, D. W. Herrmann, Monte Carlo Simulation in Statistical Physics, Springer-Verlag Berlin, 1988

[42] A. P. Young, Comput. Phys. Commun. 146, 107 (2002)